Advanced Composite Materials
Publication details, including instructions for authors and subscription information:
http://www.tandfonline.com/loi/tacm20

Experimental Investigation of Composite Sandwich Square Tubes under Quasi-Static and Dynamic Axial Crushing

Jung-Seok Kim [a] , Hyuk-Jin Yoon [b] & Kwang-Bok Shin [c]

[a] Railroad Structure Research Department, Korea Railroad Research Institute, 360-1 Woulam-Dong, Uiwang-shi, Kyunggi-do 437-757, Korea;, Email: jskim@krri.re.kr

[b] Railroad Structure Research Department, Korea Railroad Research Institute, 360-1 Woulam-Dong, Uiwang-shi, Kyunggi-do 437-757, Korea

[c] Mechanical Design Engineering, Division of Mechanical Engineering, Hanbat National University, San 16-1, Dukmyung-Dong, Yuseong-Gu, Daejon 305-719, Korea

Version of record first published: 02 Apr 2012.

To cite this article: Jung-Seok Kim , Hyuk-Jin Yoon & Kwang-Bok Shin (2011): Experimental Investigation of Composite Sandwich Square Tubes under Quasi-Static and Dynamic Axial Crushing, Advanced Composite Materials, 20:4, 385-404

To link to this article: http://dx.doi.org/10.1163/092430411X558521

VSP

Advanced Composite Materials 20 (2011) 385–404

ADVANCED COMPOSITE MATERIALS
brill.nl/acm

Experimental Investigation of Composite Sandwich Square Tubes under Quasi-Static and Dynamic Axial Crushing

Jung-Seok Kim [a,*], **Hyuk-Jin Yoon** [a] **and Kwang-Bok Shin** [b]

[a] Railroad Structure Research Department, Korea Railroad Research Institute, 360-1 Woulam-Dong, Uiwang-shi, Kyunggi-do 437-757, Korea

[b] Mechanical Design Engineering, Division of Mechanical Engineering, Hanbat National University, San 16-1, Dukmyung-Dong, Yuseong-Gu, Daejon 305-719, Korea

Received 29 March 2010; accepted 3 January 2011

Abstract

In this study, the crush behaviors of square sandwich composite tubes with woven fabric carbon/epoxy skins and aluminum honeycomb cores with the different honeycomb cell sizes and tube sizes were evaluated. For the evaluation, four different kinds of tubes were fabricated and crushed under quasi-static and dynamic impact loads. The impact tests were carried out using heavy wagons. From the test results, the crushing mode under the dynamic load was changed into more stable collapse than the corresponding static tests. Additionally, the increased bond strength between the honeycomb core and the composite face leaded to a higher energy absorption capability.

Keywords

Sandwich composite tube, honeycomb, crush, impact

1. Introduction

Reduction of the structural weight of one large component usually triggers positive synergy effects for other components. For example, a reduction of the mass of a railway car body could lead to weight savings in the traction system, suspension, brakes and other subsystems. A reduction in the total weight of railway vehicles would mean less wear on the rails, wheels and bearings, which would result in lower maintenance cost [1]. In the railway field, composites are routinely employed for the rail vehicle cabs and interior components, such as seats and paneling. In both cases, composites are primarily specified because they can be used to produce cost-effective, lightweight components of relatively complex geometries. Recently, composites have been applied for the design of the railway vehicle body structures

* To whom correspondence should be addressed. E-mail: jskim@krri.re.kr
Edited by KSCM

DOI:10.1163/092430411X558521

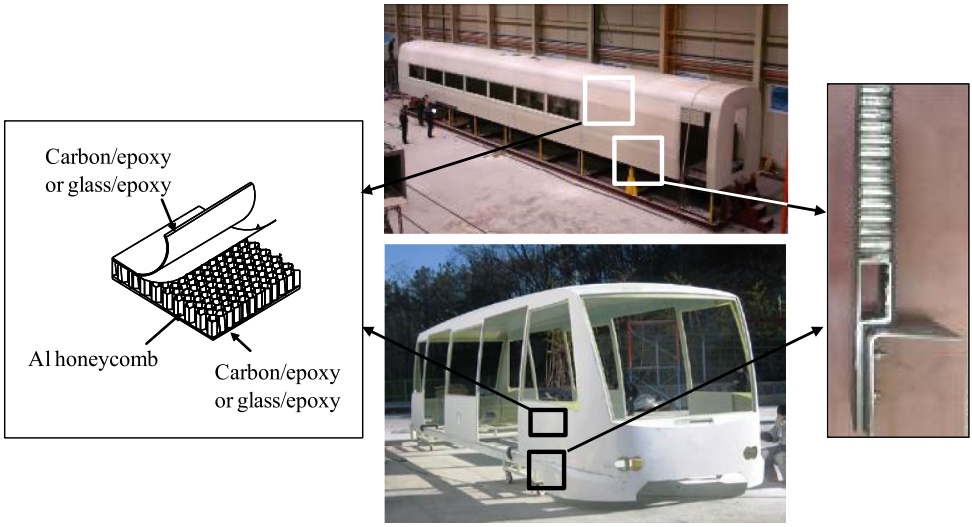

Figure 1. Railway vehicle body structures made of the sandwich composites. This figure is published in color in the online version.

because lighter vehicles would yield capacity increases [2]. In application for railway vehicle body structures, sandwich composite is usually used because of its light weight and high flexural property. Figure 1 shows railway vehicle body structures made from sandwich composites consisting of carbon/epoxy or glass/epoxy skins and aluminum honeycomb cores [3]. There are several studies on the structural behavior of sandwich composite body structures. Kim *et al.* [1, 2, 4, 5] evaluated the natural frequency of a 23-m composite train car-body by experimental and numerical simulation and studied the structural safety of the structure under static and fatigue loading conditions. However, details of the behavior of sandwich composite body structures under compressive loading have not yet been investigated. The compressive behavior of the body structure is very important to safety under collision conditions. However, the impact testing using a train body structure is extremely expensive. Particularly for a parametric study, use of small-scale models rather than large train bodies is a suitable alternative.

There have been extensive studies to evaluate the energy absorption characteristics of the composite tube structures over the last two decades. Many of these studies utilize circular or rectangular cross-section tubular specimens to determine the energy absorption capability of the material. Farley *et al.* [6–8] showed that the energy absorption capability of graphite/epoxy circular tubes was inversely proportional to fiber stiffness and that the high ultimate failure strain of graphite composites with a toughened matrix was less than the energy absorption capability of a lower failure strain system. Thornton *et al.* [9] concluded that the SEA showed a linear correlation with the tensile strength and modulus of a thermosetting resin.

In contrast to the attention paid to composite laminate tubes, studies for sandwich composite tubes have been relatively rare. Mamalis *et al.* [10–12] investigated the

axial crushing behaviors of hybrid sandwich composite rail vehicle tubular components made of foam-cored composite sandwich panels with integral FRP cylindrical energy absorbing inserts. In the study, they examined the effect of the triggering mechanism on the crash-worthiness of tested specimens. From the experimental study, they concluded that the end-crushing mode of collapse, characterized by progressive crushing initiated at one end of the shell and with failure gradually spreading along the specimen's height, was the prevalent deformation mechanism for all the structural configurations and the performance of the tulip-triggered specimen seems to be better than that of the chamfered triggered specimen, in terms of deformation.

Most of the previous studies have focused on the crush behavior of laminate tubes. Studies on the crush behavior of sandwich composites tubes have been relatively rare. In this study, to get an insight into the behavior of railway vehicle body structures made of honeycomb sandwich composites, four different kinds of square honeycomb sandwich composite tubes were manufactured under the same procedure as is used to manufacture car-body structures for the Korean tiling train, and using the same materials. The tubes were then tested under quasi-static and dynamic crush conditions. Evaluation was accomplished through a dynamic crush test carried out using impact wagons on a test track to evaluate the crush behaviors of the square sandwich composite tubes. Based on the tests, the failure modes and energy absorption capabilities of the various tubes under quasi-static and dynamic crush conditions were compared and evaluated.

2. Quasi-static and Impact Testing of Square Sandwich Composite Tubes

2.1. Preparation of Composite Tubes

Four different kinds of square sandwich composite tubes were fabricated for the experimental study as listed in Table 1. These could be divided into two groups as follows:

- tubes with cross-sectional dimensions of 300 mm × 300 mm and two different honeycomb densities of 48.6 kg/m^3 and 75.9 kg/m^3;

Table 1.
Sandwich composite tubes used in this study

Designation	Width (mm)	Height (mm)	L/W	Honeycomb cell size (mm)	Honeycomb density (kg/m^3)
T300_2_8	300	300	1	6.35 (2/8 inch)	75.9
T300_3_8	300	300	1	9.53 (3/8 inch)	48.6
T150_2_8	150	300	2	6.35 (2/8 inch)	75.9
T150_3_8	150	300	2	9.53 (3/8 inch)	48.6

- tubes with cross-sectional dimensions of 150 mm × 150 mm and two different honeycomb densities of 48.6 kg/m^3 and 75.9 kg/m^3.

The height of the tubes was 300 mm and the radius of each corner was 20 mm. The face laminates of the tubes were made of satin fabric carbon/epoxy (CF1263/RS1222) prepreg (CF1263 carbon fiber, T700 series, 12K, of Toray Industry Inc. Japan, and RS1222 resin of HFG Co. Korea). RS1222, a specially designed epoxy resin for railway vehicle body structures, includes a fire retardant. The honeycomb core made of aluminium 5052 was manufactured by the HFG Co. In all tubes, the thickness of the honeycomb core was 10 mm and the thicknesses of the inner face and outer face were 1.5 mm and 3 mm, respectively. The carbon/epoxy faces and the honeycomb core were bonded using BONDEX® 606 adhesive film (HFG Co. Korea). The fiber volume fraction of the composite face was 64.1%.

Table 2 shows the material properties of the CF1263 woven fabric carbon/epoxy. The stacking sequence of the tube was (warp/fill/warp/aluminum honeycomb/fill/warp)$_T$. The warp direction of the woven fabric and the ribbon direction of the honeycomb core were aligned with the axial direction of the tube.

To fabricate the sandwich composite tube, two kinds of steel moulds with cross-sectional dimensions of 150 mm × 150 mm and 300 mm × 300 mm were manufactured as shown in Fig. 2(a). Then, the inner face was laid up to the target thickness of 1.5 mm. After the lay-up of the inner face, it was sealed and pressured using a vacuum bag. Next, it was cured in an autoclave under the curing cycle shown in Fig. 3. After the curing of the inner face, the honeycomb core, the adhesive film and the prepreg for the outer face were stacked in sequence. Figure 2(b)–(e) shows the lay-up sequence to fabricate the sandwich composite tubes. Figure 2(f) shows the final shape and dimension of the square sandwich composite tubes. To allow a realistic simulation of the railway vehicle body, no trigger mechanisms were introduced into the tubes.

2.2. *Quasi-static and Dynamic Impact Tests*

Quasi-static crushing tests were performed in a 3000 kN capacity hydraulic loading machine. Load platens were set parallel to each other prior to initiation of the tests. All tubes were compressed to 200 mm and the loading rate was 10 mm/min. The load–displacement of the cross-head was recorded by an automatic data acquisition system.

For the dynamic impact tests, a 4-axle crash tank wagon and a 4-axle flat wagon were used. The impact wagons were accelerated and shunted by a V22 locomotive in order to bump into the specimen to be tested. The crash tank wagon of Fig. 4(a) is filled with concrete and weighs approximately 760 kN. The 4-axle flat wagon of Fig. 4(b) weighs approximately 230 kN and can be used for testing at higher impact speeds in order to reach the same amount of energy. The deformation path over the crash tubes and the actual impact speed were measured. The impact force was measured by three load cells of 2 MN capacity installed behind the adapter plate,

Table 2.
Quasi-static and dynamic impact test results for composite sandwich tubes

Tube types	Strain rate	Max. load (kN)	Mean load (kN)	CFE (%)	Crushed displacement (mm)	Collapse mode	SEA (kJ/kg)	Impactor types
T300_3_8	Quasi-static	1789.5	313.2	17.5	200	Unstable local buckling	14.2	–
	3.15 s^{-1}	772	323	37.9	92	Splaying	6.74	76-ton tank train
	4.17 s^{-1}	596	151	23.3	245	Splaying	8.39	76-ton tank train
T300_2_8	Quasi-static	1847.2	394.3	21.3	200	Mixed mode	15.8	–
	3.15 s^{-1}	962	321.7	30.8	135	Splaying	9.73	76-ton tank train
	3.15 s^{-1}	893	258	28.9	155	Splaying	8.03	76-ton tank train
T150_3_8	Quasi-static	828.3	266.7	32.2	200	Splaying	23.0	–
	2.41 s^{-1}	577	209	32.6	83	Splaying	7.48	76-ton tank train
	2.78 s^{-1}	590	216	32.4	111	Splaying	10.3	76-ton tank train
	5.28 s^{-1}	502	177	25.8	240	Splaying	18.3	76-ton tank train
T150_2_8	Quasi-static	778.1	373.3	48.0	200	Splaying	27.9	–
	3.61 s^{-1}	390	282	64.0	39	Tube wall collapsing inward	4.10	23-ton flat wagon
	6.02 s^{-1}	409	298	58.2	105	Tube wall collapsing inward	11.7	23-ton flat wagon

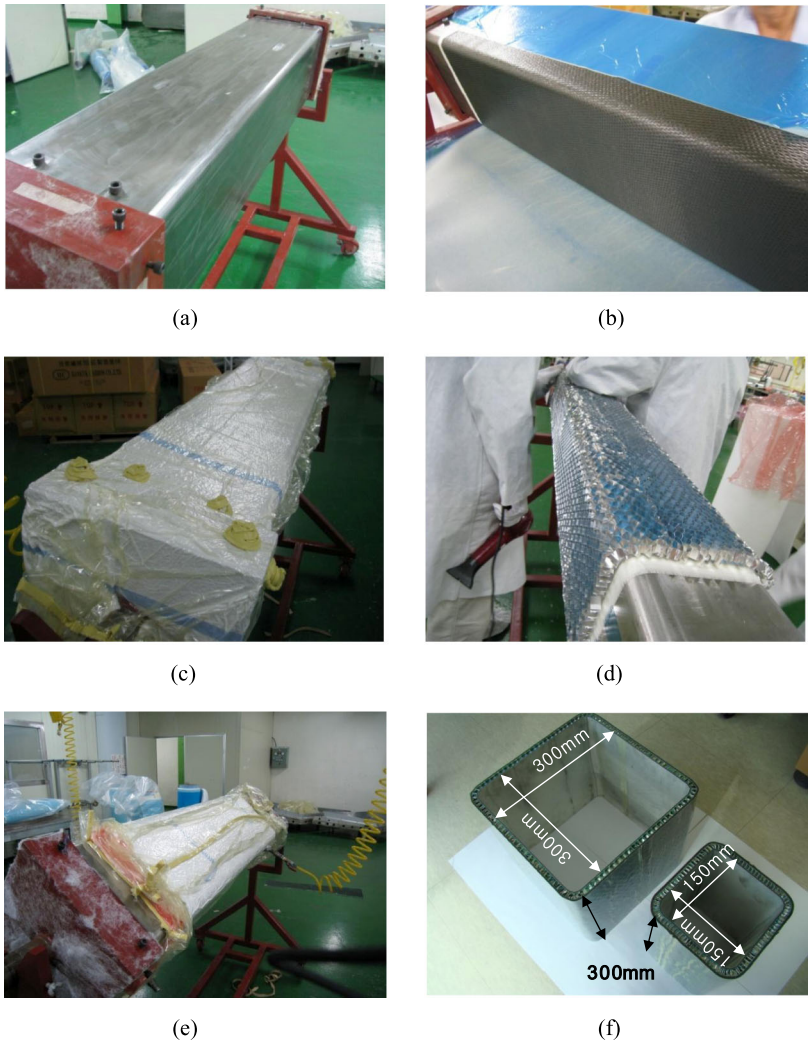

Figure 2. Manufacturing process of the composite sandwich tube structure: (a) steel mould; (b) lay-up of inner wall; (c) vacuuming process; (d) stacking of aluminium honeycomb core; (e) the vacuum bagged structure for the autoclave curing; (f) the cured square sandwich composite tubes. This figure is published in color in the online version.

as shown in Fig. 4(c). The square sandwich composite tubing was installed on the adapter plate using a specially designed fixture to prevent separation under dynamic load (Fig. 4(d)).

The deformation path over the crash tube corresponds to the total displacement and was measured at the wagon by means of a ruler. The impact force–displacement data were acquired under the measuring frequency of 10 kHz. The impact speed was measured immediately before the impact using a speed measuring device and the test was recorded at 1000 frames/s by means of a high speed camera so that

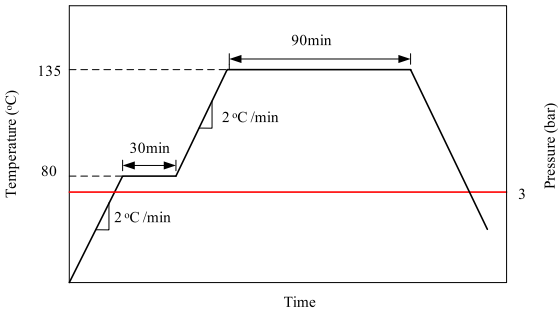

Figure 3. Curing cycle for the composite sandwich tube. This figure is published in color in the online version.

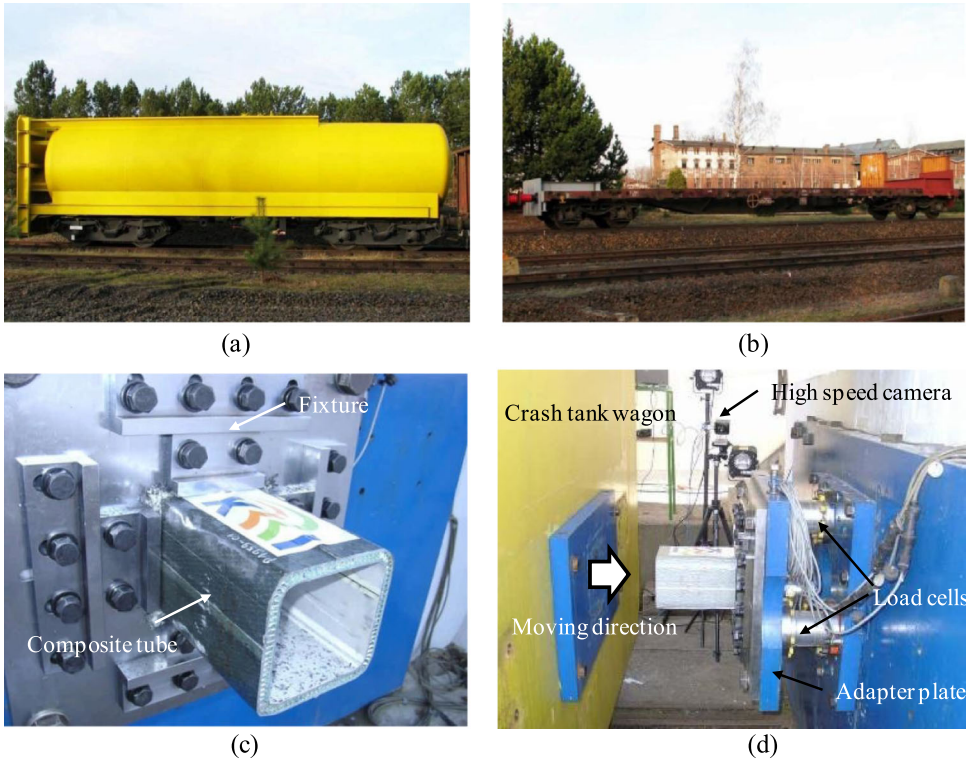

Figure 4. Setup for the dynamic impact test: (a) 4-axle flat wagon; (b) 4-axle crash tank wagon; (c) fixture to install the tube; (d) experimental apparatus of the dynamic impact test. This figure is published in color in the online version.

the failure modes could be examined in detail. The measured data were filtered by means of a 4th order Butterworth low pass filter, 180 Hz, according to ERRI B 12/Rp17, Annex K [13].

Two tube specimens per each size were used for the static test, while one tube specimen per each size was used for the impact test for each strain rate due to the limited specimens.

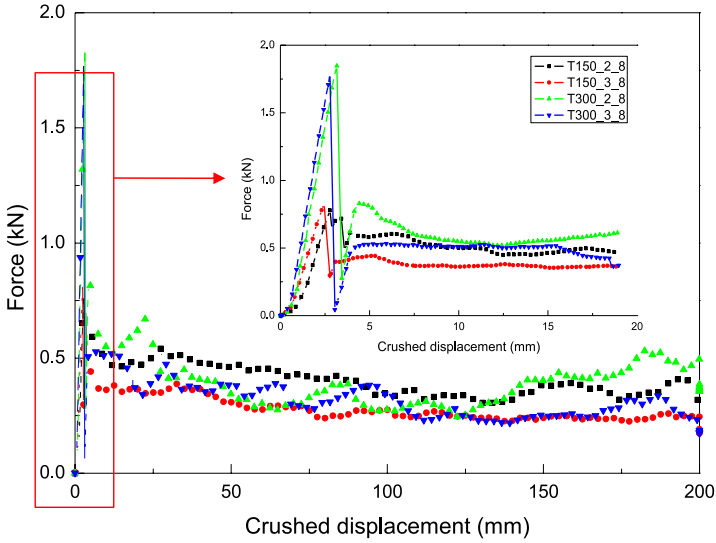

Figure 5. Load–displacement curves under the quasi-static load. This figure is published in color in the online version.

3. Results and Discussion

3.1. Load–Displacement

Figure 5 shows the load–displacement curves for the four kinds of tube subjected to quasi-static axial crushing. The initial peak loads of the T300 tubes were two times greater than those of the T150 tubes. After the peak load, the load histories of the T300 tubes were followed by abrupt load drops: in the case of the T300_3_8 tube, the load dropped nearly to zero. In all T300 tubes, the post-crushing region of the load–deflection curve was characterized by higher fluctuated behavior than the T150 Tubes due to the tube wall buckling as shown in Fig. 5.

The T300_3_8 tube was crushed, accompanied by buckling of the tube wall. This was caused by the low ratio of wall span and height ($L/H = 1.0$) of the tubes. Figure 6(a) presents the typical crushing process of the T300_3_8 tube. The axial load increased initially and micro-fragmentation was observed. The maximum load, $P_{\max}$, was attained in the first 2.84 mm of compression (see Fig. 6(a)). After maximum load, the load dropped rapidly and then the tube wall expanded outward (see ① of Fig. 6(a)). With the platen moving downward, the large area of the tube wall buckled convexly (see the dashed line of ② of Fig. 6(a)). The tube then collapsed, with formation of hinges accompanying the concave wall buckling (see the dashed line of ③ of Fig. 6(a)), followed by a gentle load drop. Unlike the T300_3_8 tube, the crushing behavior of the T300_2_8 tube was relatively stable, without buckling.

Although the tubes have no trigger mechanism, the T150_3_8 and T150_2_8 tubes showed the splaying mode of collapse, characterized by progressive crushing

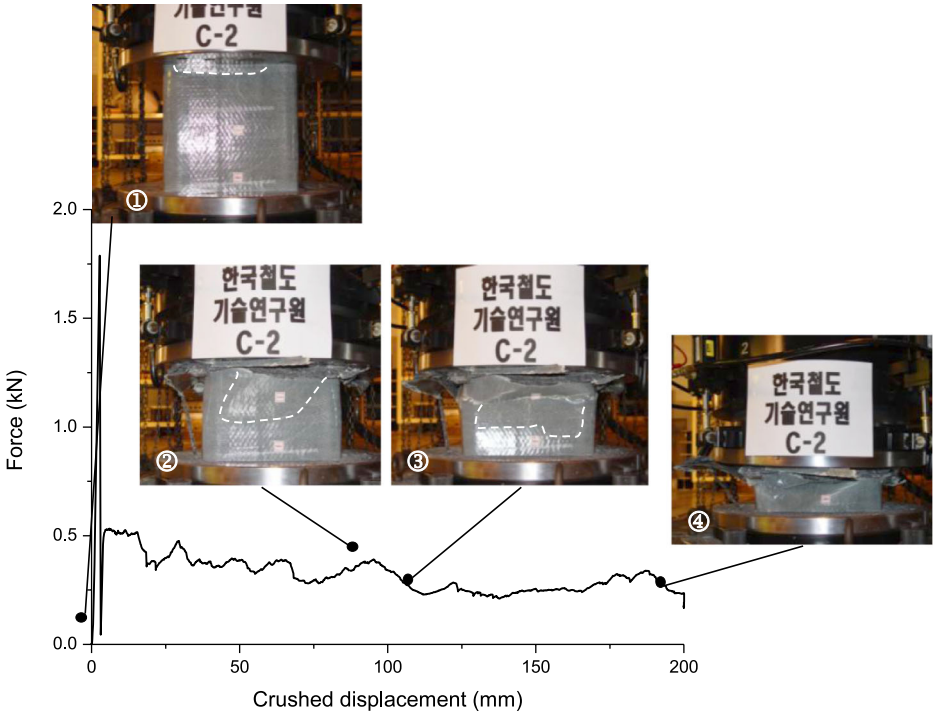

(a)

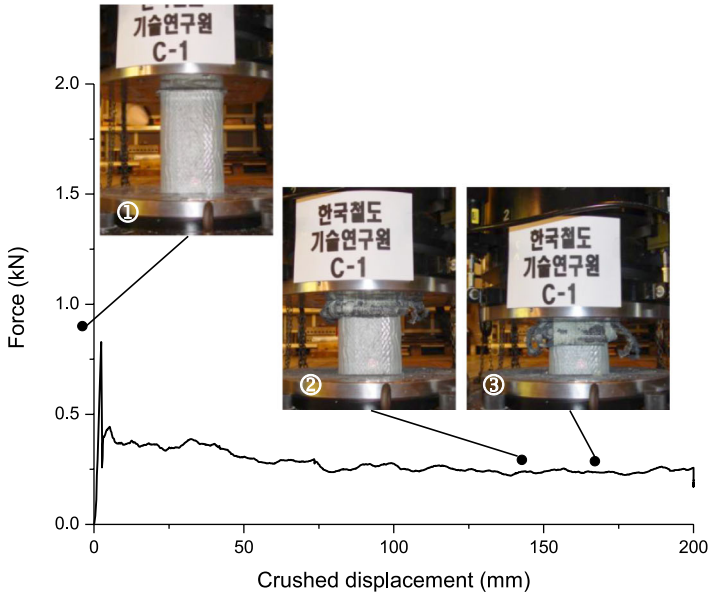

(b)

Figure 6. Crushing process of T300_3_8 and T150_3_8 tube under quasi-static axial compression: (a) T300_3_8 tube; (b) T150_3_8 tube. This figure is published in color in the online version.

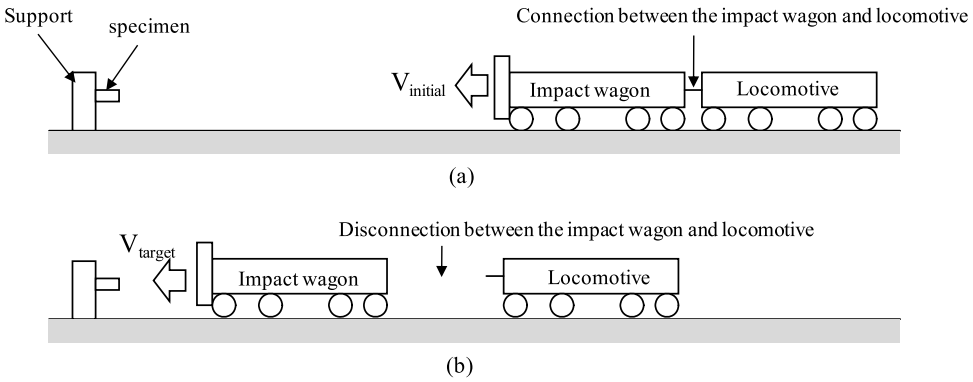

Figure 7. Schematic diagram for the dynamic crush test using the impact wagon: (a) the acceleration of an impact wagon by the V22 locomotive; (b) disconnection between the locomotive and the impact wagon.

initiated at one end of the shell and failure gradually spreading along the specimen's height. Figure 6(b) presents the typical crushing process of the T150_3_8 tube.

As mentioned before, a 23-ton flat wagon and a 76-ton tank train were used for the dynamic crush tests. The impact wagon was first accelerated by the V22 locomotive (Fig. 7(a)) and was then disconnected from the locomotive when it was at an appropriate speed and at an appropriate distance from the specimen (Fig. 7(b)). Unlike when using laboratory test facilities, it is hard to control an impact wagon so that it runs at a target speed on a real test track. Therefore, there were several pre-shunting tests to determine the appropriate shunting speed and distance necessary to meet the target crushing speed. All of the tubes except the T150_2_8 tube were impacted using the 76-ton tank train. Only the T150_2_8 tube was impacted by the 23-ton flat wagon. Figure 8 presents the load–displacement curves of each tube at different strain rates. In the case of tubes impacted by the 76-ton tank train (Fig. 8(a)–(c)), the initial peak loads and the mean crush loads were decreased with the increased strain rate, while the crushed length was increased. In the case of tubes impacted by the 23-ton flat wagon (Fig. 8(d)), in contrast, the initial peak loads, the mean loads, and the crushed length were increased with the increased strain rate.

Figure 9 shows the dynamic crushing process of the T300_3_8 tube at the strain rate of 4.17 s^{-1} and the T150_3_8 tube at the strain rate of 5.28 s^{-1}.

3.2. Collapse Modes and Failure Mechanisms

Four distinct modes were observed in the series of static and dynamic axial compression tests of the sandwich composite square tubes. The concurrence of different collapse modes on the same test specimen is attributed to lack of uniformity in the structure of the laminate material along the four sides of the square tubes and especially at the corners.

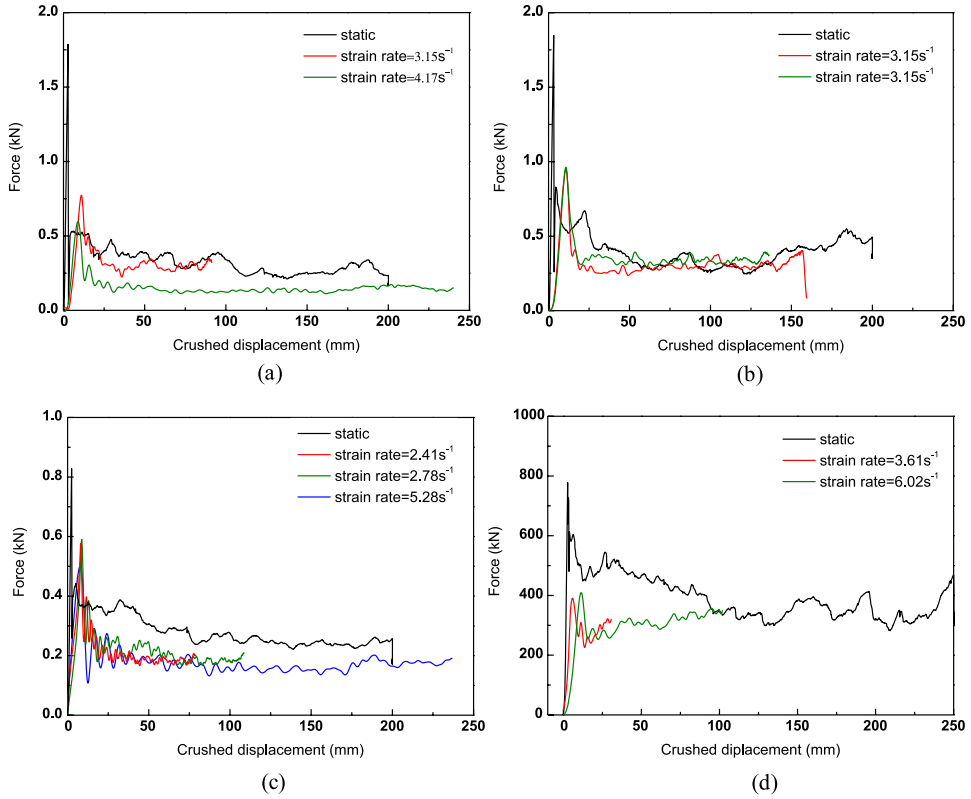

Figure 8. Load–displacement curves under the dynamic load conditions. (a) T300_3_8 tube; (b) T300_2_8 tube; (c) T150_3_8 tube; (d) T150_2_8 tube. This figure is published in color in the online version.

3.2.1. Wall Buckling Mode

The wall buckling mode was characterized by unstable local tube wall buckling on all four tube sides and transverse failure of the FRP walls. The mode was observed only during the static axial compression test of the T300_3_8 tube (Fig. 10(a)). The tube wall buckling was initiated after the maximum load and was followed by a drastic load drop. During the wall buckling process, the faces and honeycomb core debonded, and the inner and outer face sheets were deformed convexly and concavely as hinges formed in the material (Fig. 10(a)). As a result of the hinge formation and bending force induced by the loading platen, many transverse fractures occurred in the tube wall (Fig. 10(a)). Consequently, in the post-buckling region of specimens that collapsed according to the wall buckling mode, the mean crushing load was much lower than the peak load.

The main failure mechanisms that contribute to energy dissipation in the wall buckling mode are the following:

- Buckling of the tube walls;

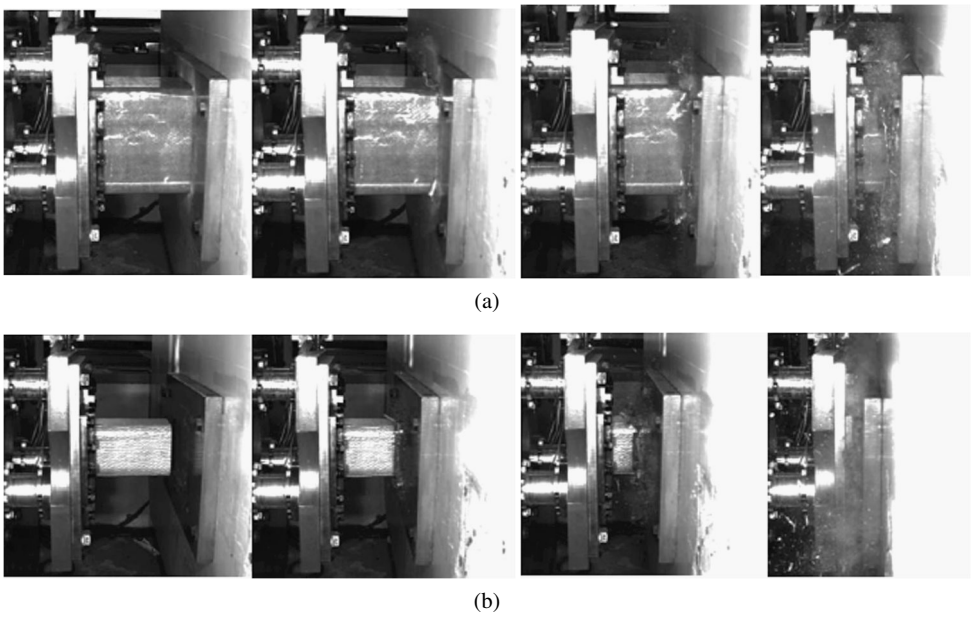

Figure 9. Crushing process of T300_3_8 and T150_3_8 tube under dynamic axial compression: (a) T300_3_8 tube; (b) T150_3_8 tube.

- Transverse fracture, crack propagation and axial splitting of the tube corners;
- Debonding between the faces and honeycomb core;
- Bending and flexural damage of the fractured tube walls;
- Sliding of the fractured tube walls against the steel crossheads under frictional resistance.

3.2.2. Splaying Mode

The splaying mode was characterized by progressive end-crushing of the axially compressed tube, the formation of two continuous fronds per tube side which spread outwards and inwards, splitting of the square tube at its corners, and high absorption of crash energy. At the initial stages of the crushing, four axial cracks were formed at the corners of each tube which caused bending of the internal and external fronds. It was observed that the external fronds were longer than the internal fronds. No axial tear was observed during the crush process. This mode was observed in the case of all dynamic compression tests of the T300 and T150 (Figs 11 and 12(a)) tubes, with the exception of the T150_2_8 tube and the static axial compression tests of the T150 tube (Fig. 10(c)–(d)). That is, the splaying mode was observed in approximately 77.8% of the dynamic axial compression tests but in only 25% of the static tests. This result means that the increase of the compressive strain rate tends to result in the stable collapse of the CFRP tubes. With respect to the

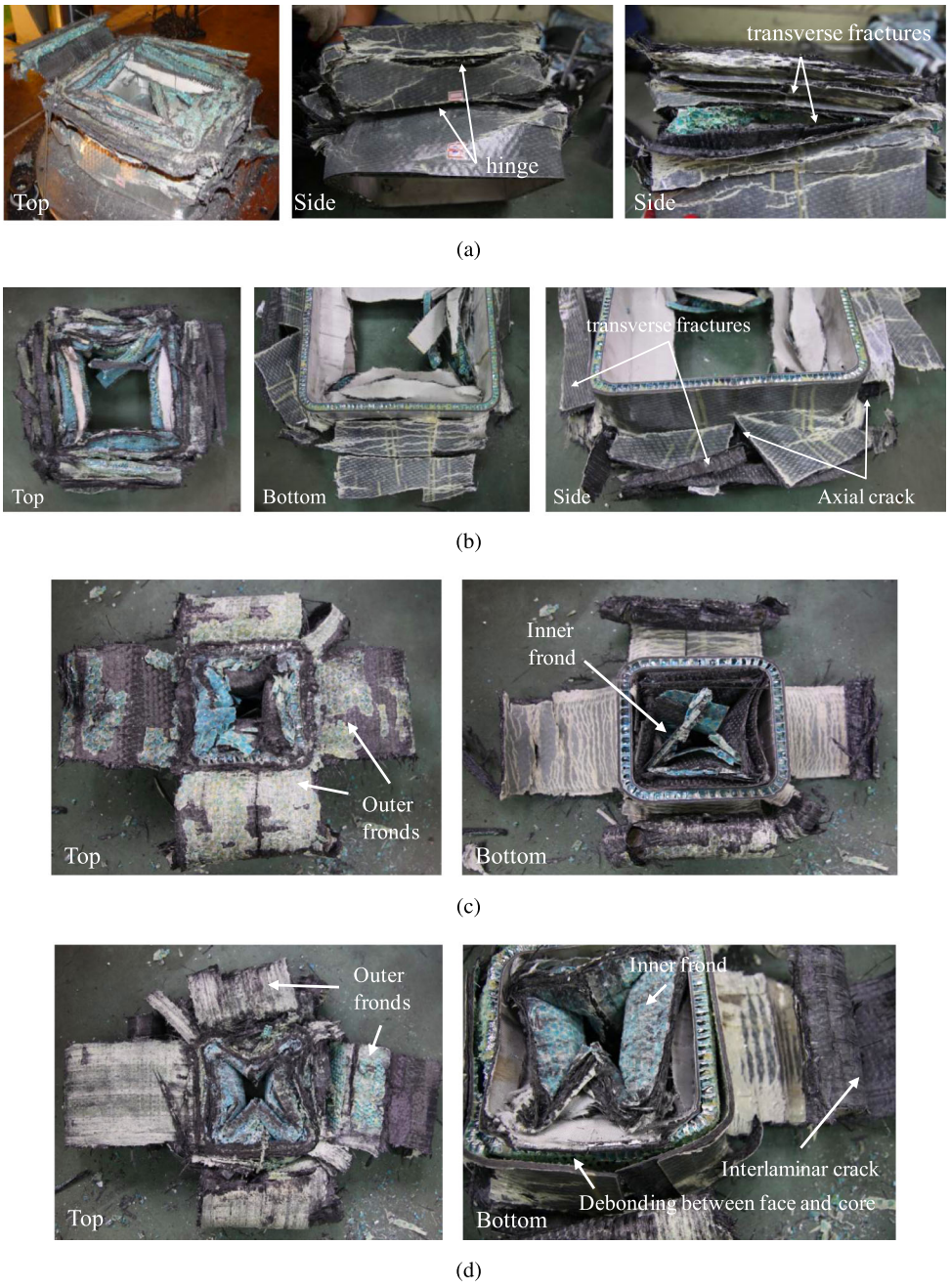

Figure 10. Final shapes of the statically compressed tubes: (a) T300_3_8 tube; (b) T300_2_8 tube; (c) T150_3_8 tube; (d) T150_2_8 tube. This figure is published in color in the online version.

aspect ratio, L/W, 71.4% of the T150 tube samples, which had aspect ratio of 2, collapsed according to splaying mode, while only 66.7% of the T300 tube was

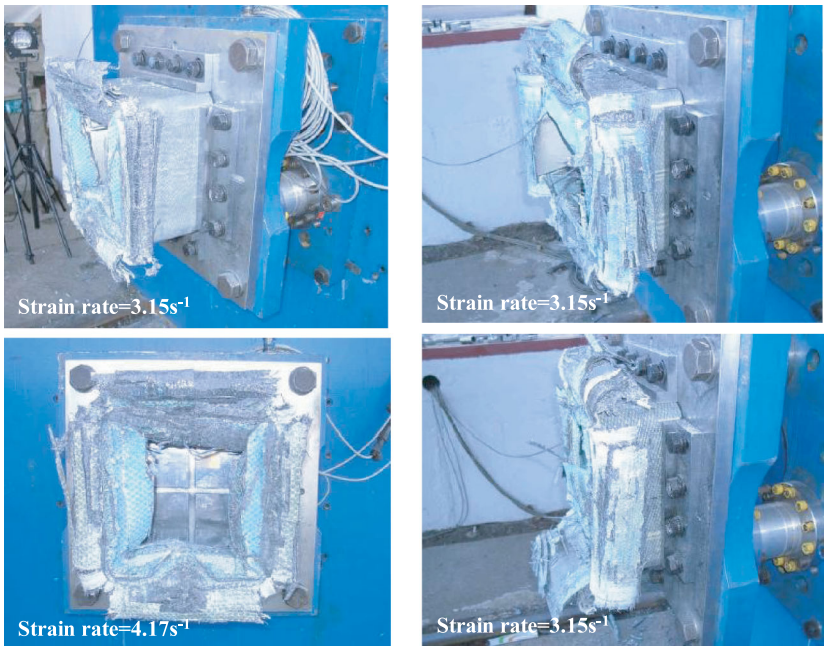

Figure 11. Final shapes of the dynamically compressed tubes at different strain rates: (a) T300_3_8 tube; (b) T300_2_8 tube. This figure is published in color in the online version.

similarly affected. Severe interlaminar cracking occurred between adjacent plies of the outer fronds, as shown in Figs 10(d), 11(b) and 12(a). In this mode, with increasing compression load, the walls of the honeycomb core that was bonded between the inner face and outer face deformed and started touching each other, and the core reached nearly total compaction. Simultaneously, the honeycomb core was debonded from the inner face and outer face of the tube. The totally compacted honeycomb core played the role of a wedge axially through the tube wall between the laminate faces, as shown in Fig. 13. Figure 13 shows a sectional view (A–A section of Fig. 13(c)) of the T150_2_8 tube under static (Fig. 13(a)) and dynamic loads (Fig. 13(b)).

From the analysis of the tube deformation behavior, it may be concluded that energy dissipation for the splaying mode is effected mainly by the following failure mechanisms:

- Axial splaying of the tube walls;
- Penetration through the two tube faces under high frictional and debonding resistance from a debris wedge formed of the fully compressed honeycomb core;
- Bending of the fronds and flexural damage of the reinforcing plies of the lamina bundles;

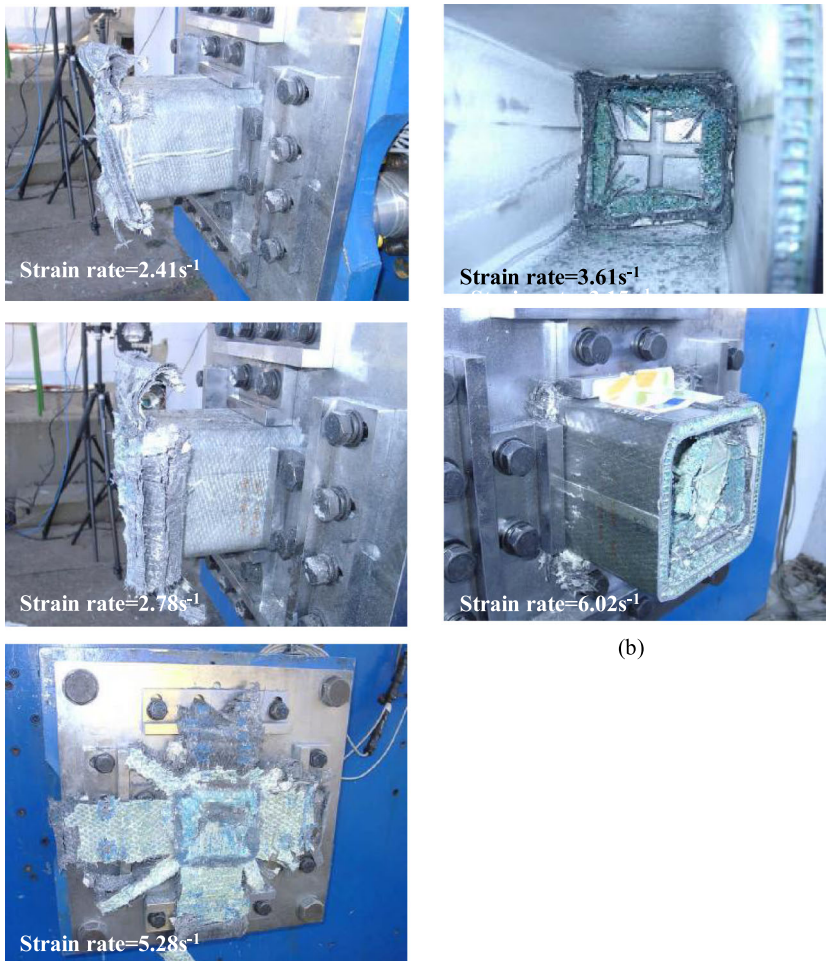

Figure 12. Final shapes of the dynamically compressed tubes at different strain rates: (a) T150_3_8 tube; (b) T150_2_8 tube. This figure is published in color in the online version.

- Transverse fracturing, crack propagation and axial splitting of the tube corners;
- Sliding of the external and internal fronds against the crosshead under high frictional resistance.

3.2.3. Mixed Mode of Splaying and Fragmentation

There was a mixed mode characterized by a combination of splaying and fragmentation modes. The fragmentation mode was characterized by a wedge-shaped laminate cross section with one or multiple short interlaminar and longitudinal cracks. This mode was observed only in the case of the static axial compression test of T300_2_8 tube (Fig. 10(b)).

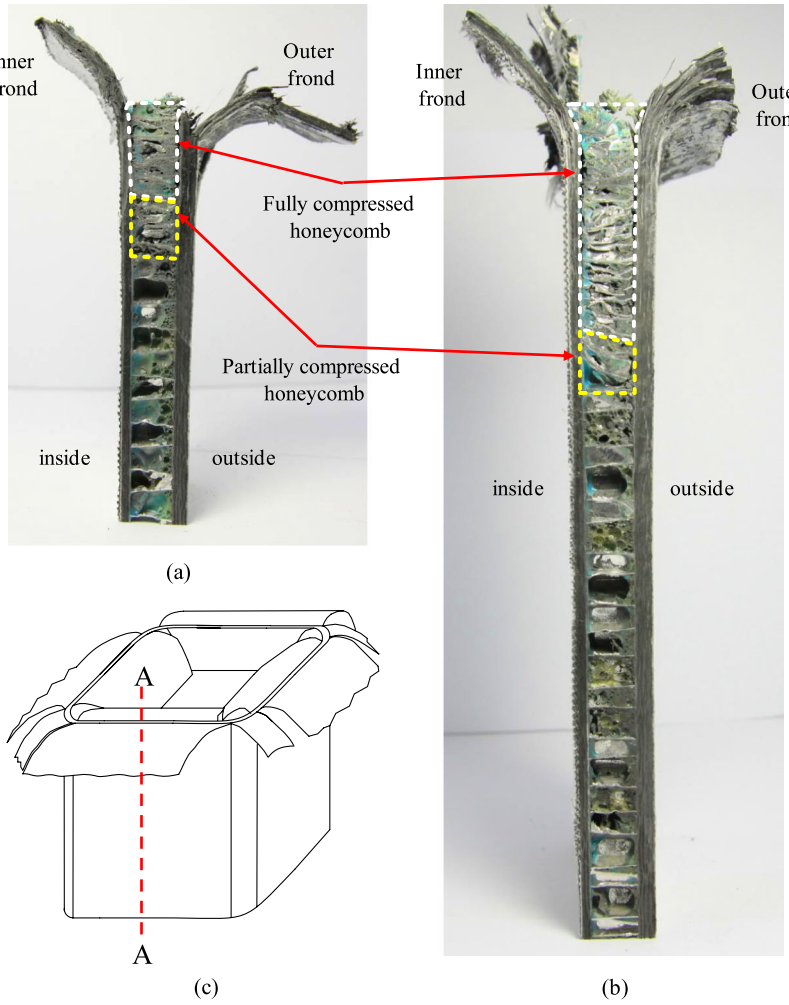

Figure 13. The sectional view of the T150_2_8 tube: (a) static load; (b) dynamic load; (c) section definition. This figure is published in color in the online version.

Under this mode, the tube started to collapse by splaying mode and, with further deformation, transverse fractures of the tube wall and longitudinal cracks at both the corners and at centers of the sides developed (Fig. 10(b)).

The main failure mechanisms that contribute to energy dissipation for the mixed mode are as follows:

- Axial splaying of the tube walls;
- Penetration through the two tube faces under high frictional and debonding resistance from a debris wedge formed by the fully compressed honeycomb core;

- Bending of the fronds and flexural damage of the reinforcing plies of the lamina bundles;
- Delamination of the bent fronds and sliding between adjacent plies under high frictional resistance;
- Sliding of the external and internal fronds against the crosshead under high frictional resistance.

3.2.4. Mode of Tube Wall Collapsing Inward into the Tube Inside

This final mode was characterized by the progressive inward collapse of the tube without any formation of fronds, and by the splitting of the square tube at its corners. This mode was observed only in the case of the dynamic axial compression test of the T150_2_8 tube (Fig. 12(b)). As mentioned before, that tube was the only tube crushed by the 23-ton flat wagon. The collapsed tube wall was compacted inside of the tube as shown at the bottom of Fig. 12(b). Facial fracturing and debonding between the faces and the honeycomb core were observed in the compacted tube wall.

The main failure mechanisms that contribute to energy dissipation for the collapsing tube wall mode are as follows:

- Inward bending of the tube walls;
- Debonding between the faces and the honeycomb core;
- Bending and flexural damage of the fractured tube walls;
- Sliding of the bent tube walls against the steel crossheads under frictional resistance.

3.3. Energy Absorption Characteristics

In this study, the energy absorbing capability was estimated by following parameters.

- Specific energy absorption (SEA): to compare different materials or different geometry of specimens, it is necessary to consider the specific energy. The specific energy is defined as the amount of energy absorbed per unit mass crushed material:

$$\mathrm{SEA} = \frac{P_\mathrm{m}}{A_\rho} \cdot \frac{L_\mathrm{c}}{h}, \tag{1}$$

where P_m is the mean crush load, A is cross-sectional area of the tube, ρ is the density of the tube, h is the height of the tube and L_c is the crushed length of the tubes.

- Crush force efficiency (CFE): CFE is the ratio between the mean crush load, P_m and the initial peak load, P_{max}. It is useful to measure the performance of an absorber. It can be calculated as:

$$\mathrm{CFE} = \frac{P_m}{P_{max}}. \tag{2}$$

These parameters were investigated as listed in Table 2.

In the quasi-static load cases, the tubes with a denser honeycomb core and higher aspect ratio showed a higher SEA. This trend was the same in the CFE. The tubes collapsed with the wall buckling mode had a minimum CFE and the lowest SEA in all the test specimens as listed in Table 2. In all types of tubes, the SEA measured from the dynamic tests showed the decreasing trend compared with the static one while the CFE of the dynamic tests was higher than the corresponding static tests.

3.3.1. Effect of Strain Rate

In all kinds of tubes, generally, the specific energy absorption (SEA) showed an increasing trend with the strain rate. This trend was opposite to the mean crush load. The reason for this was that the crushed length was increased with the strain rate. However, the SEA under the dynamic tests was lower than that of the corresponding static tests.

Particularly, the three kinds of tubes of T300_3_8, T300_2_8, and T150_2_8 showed different crushing modes under the static and the dynamic load conditions. In the case of the T300 tubes, the crushing mode under the dynamic load was changed into a more stable type than with the corresponding static tests. The T150 tubes maintained the stable mode under both the static and the dynamic load conditions, although the mode of the T150_2_8 changed from the splaying mode to the tube wall collapsing inward mode.

The crushing force efficiencies under the dynamic load conditions decreased with the strain rate.

3.3.2. The Effect of Tube Geometry and Bond Strength between the Composite Skin and the Honeycomb Core

Because the compressed tubes were constructed using the same combination of constituent materials, the effect of tube geometry (especially, the aspect ratio, L/W) and of the bond strength between the composite skin and the honeycomb core was investigated. In terms of tube geometry, tubes with a larger aspect ratio showed a higher energy absorption capability in both load conditions.

In order to investigate the bond strength effect, the bond strength between the honeycomb core and the composite face was measured by a drum peel test based on ASTM D1781 [14] as shown in Fig. 4. That test method assesses the peel resistance of adhesive bonds between a relatively flexible adherend and a rigid adherend; in this case, between the relatively flexible facing of a sandwich structure and its core [14].

Figure 14. Drum peel test for the composite sandwich plates. This figure is published in color in the online version.

In the test, the average peel torque (T) calculated by equation (3) was measured:

$$T = \frac{[(r_o - r_i)(F_p - F_o)]}{W}, \tag{3}$$

where T is the average peel torque along the width, r_o is the radius of the flange, r_i is the radius of the drum plus one-half the thickness of the adherend being peeled, F_p is the average load required to bend and peel the adherend plus the load required to overcome the resisting torque, F_o is the load required to overcome the resisting torque and W is the width of the specimen. Further details of the test can be found in the ASTM D 1781 [14].

The average peel torques of the honeycomb cores with densities of 75.9 kg/m^3 and 48.6 kg/m^3 were 1490 mm · N/76.2 mm and 1017 mm · N/76.2 mm, respectively. The honeycomb core with a density of 75.9 kg/m^3 has a bond strength that is 46.5% higher than that with a density of 48.6 kg/m^3. The tube with the denser honeycomb core had a higher energy absorption capability due to the increased bond strength between the honeycomb core and the composite face, which results from the wider bonding area.

4. Conclusions

Our comparison of the crash-worthiness of various square sandwich composite tubes under static and dynamic crushing leads to the following conclusions:

(1) The crushing mode of the tubes tested could be categorized into four different modes; unstable local buckling mode, mixed mode of splaying and fragmentation, progressive end crushing mode, and tube wall collapsing inward mode.

(2) The tubes under the quasi-static load conditions showed a higher specific energy absorption capability than the impact load conditions.

(3) Under the dynamic crushing conditions, the SEA increased with the strain rate while the mean crushing loads decreased. The load condition change from the static to the dynamic makes the crushing mode more stable.

(4) Increased bond strength between the honeycomb core and the composite face resulted in a higher energy absorption capability.

References

1. J. S. Kim and J. C. Cheong, Natural frequency evaluation of a composite train carbody with length of 23 m, *Compos. Sci. Technol.* **66**, 2272–2283 (2006).
2. J. S. Kim, J. C. Cheong and S. J. Lee, Numerical and experimental studies on the deformational behavior of a composite train car-body of the Korean tilting train, *Compos. Struct.* **81**, 225–241 (2006).
3. http://hc.fiber-x.com/
4. J. S. Kim, S. J. Lee and K. B. Shin, Manufacturing and structural safety evaluation of a composite train car-body, *Compos. Struct.* **78**, 468–476 (2007).
5. J. S. Kim, J. C. Cheong, S. J. Lee, S. H. Cho, S. H. Yoon, S. H. Han and S. L. Seo, Structural safety evaluation of the hybrid composite body-shell for Korean tilting train by a whole body test, *Key Engng Mater.* **331**, 334–335 (2007).
6. G. L. Farley, Energy absorption of composite materials, *J. Compos. Mater.* **17**, 267–279 (1983).
7. G. L. Farley, Effect of fiber and matrix maximum strain on the energy absorption of composite materials, *J. Compos. Mater.* **20**, 322–334 (1986).
8. G. L. Farley, R. K. Bird and J. T. Modlin, The role of fiber and matrix in crash energy absorption of composite materials, *J. Amer. Helicopter Soc.*, April, pp. 52–58 (1989).
9. P. H. Thornton and R. A. Jeryan, Crash energy management in composite automotive structures, *Intl J. Impact Engng* **7**, 167–180 (1988).
10. A. G. Mamalis, D. E. Manolakos, G. A. Demosthenous and M. B. Ioannidis, *Crashworthiness of Composite Thin-walled Structural Components*. CRC Press, New York, USA (1998).
11. A. G. Mamalis, D. E. Manolakos, M. B. Ioannidis and P. K. Kostazos, Axial crushing of hybrid square sandwich composite vehicle hollow bodyshells with reinforced core: experimental, *Intl J. Crash* **6**, 363–376 (2001).
12. A. G. Mamalis, D. E. Manolakos, M. B. Ioannidis, P. K. Kostazos and D. P. Papapostolou, Axial collapse of hybrid square sandwich composite tubular components with corrugated core: numerical modeling, *Compos. Struct.* **58**, 571–582 (2002).
13. European Rail Research Institute B 12/RP 17, Annex K, 7th edn (1993).
14. ASTM D 1781-98. Standard test method for climbing drum peel for adhesives. Annual book of ASTM standards. West Conshohocken, PA: ASTM (2004).